Variability of Fram Strait Ice Flux and North Atlantic Oscillation

R. Kwok and D. A. Rothrock*

Jet Propulsion Laboratory
California Institute of Technology
4800 Oak Grove Dr
Pasadena, CA 91109

* *Polar Science Center, Applied Physics Laboratory*
College of Ocean and Fisheries Sciences
University of Washington
Seattle, WA 98195

Submitted to JGR-Oceans
April, 1998

Corresponding author:
Ron Kwok
MS 300-235
Jet Propulsion Laboratory
4800 Oak Grove Dr
Pasadena, CA 91109
Ph. (818) 354-5614
FAX: (818) 393-3077
email:ron@rgps1.jpl.nasa.gov

Variability of Fram Strait Ice Flux and North Atlantic Oscillation

R. Kwok and D. A. Rothrock

Abstract

We estimate the winter sea ice export through the Fram Strait using ice motion from satellite passive microwave data. Sea ice motion (October through May) is obtained by tracking the displacement of common features in sequential 85 GHz and 37 GHz brightness temperature fields. The average winter area flux over the 18-year record (1978-1996) is 670,000 km^2, approximately 7% of the area of the Arctic Ocean. The winter area flux ranges from a minimum of 450,000 km^2 in 1984 to a maximum of 906,000 km^2 in 1995. The daily, monthly and interannual variabilities of the ice area flux are high. There is an upward trend in the ice area flux over the 18-year record. The average winter volume flux over the winters of Oct 1990 through May 1995 is 1745 km^3 ranging from a low of 1375 km^3 in 1990 flux to a high of 2791 km^3 in 1994. The sea-level pressure gradient across the Fram Strait explains more than 80% of the variance in the ice flux over the 18-year record. We use the coefficents from the regression of the time-series of area flux versus pressure gradient across the Fram Strait and ice thickness data to estimate the summer area and volume flux. The average 12-month area flux and volume flux are 919,000 km^2 and 2366 km^3. We find a significant correlation (R =0.86) between the area flux and positive phases of the North Atlantic Oscillation (NAO) index over the months of December through March. Correlation between our six years of volume flux estimates and the NAO index gives R =0.56. During the high NAO years, a more intense Icelandic low increases the gradient in the sea-level pressure by almost 1 mbar across the Fram Strait thus increasing the atmospheric forcing on ice transport. Correlation is reduced during the negative NAO years because of decreased dominance of this large-scale atmospheric pattern on the sea-level pressure gradient across the Fram Strait.

1. Introduction

The present examination of ice flux through Fram Strait pertains to a much larger problem: the episodic freshening of the surface waters of the Greenland and Labrador seas and the control these events have on the global ocean thermohaline circulation [*Dickson et al.*, 1988]. This freshening is caused by anomalous outflows from the Arctic Ocean of surface freshwater and sea ice. The budget presented by *Aagaard and Carmack* [1989] lists ice flux through Fram Strait as the largest single component of the Greenland-Iceland-Norwegian (GIN) Sea freshwater balance. The important role of the this flux is well established, even though its magnitude is still in question. Estimates purporting to give a mean volume flux through Fram Strait vary from 1900 to 5000 $km^3\ yr^{-1}$ (0.06 to 0.16 Sv) as reviewed below. The range of area flux estimates is smaller.

To estimate the volume flux one ideally would want time dependent profiles across the strait of the normal component of velocity and of ice thickness. Both have proven difficult to obtain. Climatological velocity profiles have been extracted from drifting buoy data [*Vinje and Finnekasa*, 1986; *Moritz*, 1988] and seasonal profiles have been extracted from AVHRR [*Martin*, 1996]. Ice draft data continue to be the most sparse; those obtained from submarine sonar data give some cross-strait variations [*Wadhams*, 1983; *Vinje and Finnekasa*, 1986] and those obtained more recently from moored sonars resolve six years of temporal variability [*Vinje et al.*, 1998].

What makes observing this ice flux so difficult is the very property needed to relate it to climate change: its temporal variability. Because thickness observations are so difficult to obtain, models probably offer the best insight into how the variability of ice thickness contributes to the variability of volume flux. In a box model calculation driven by velocities, *Thomas et al.* [1996] found that the annual average ice flux of 1900 $km^3\ yr^{-1}$ varied over a range of about 2000 $km^3\ yr^{-1}$ (0.06 Sv), and that 90% of the variance of volume flux is attributable to variability of

velocity. By comparison, the variability in the ocean component of freshwater outflow is probably relatively small; examinga box model over a seven year period, *Steele et al.* [1996] estimate that the freshwater outflow of 0.024 Sv varies by about 0.003 Sv (90 km^3 yr^{-1}). There is also considerable variability in the north-south direction along the direction of flow. The ice appears to diverge as it flows southward through the strait. The different lines across which the flux has been estimated accounts for some of the differences between estimates by different investigators.

These variations are tied to climate. Several authors have noted the variability of the arctic surface pressure field and its relation to variations in ice motion with the Arctic basin and through Fram Strait. *Serreze et al.* [1992] surmise that anomalies in surface pressure and winds that drive ice motion would cause variations in the amount of multiyear ice in the Fram Strait ice flow. *Walsh et al.* [1996] point out the weakening of the Arctic anticyclone since 1988; the high pressure has dropped by 5 mb from 1979-1986 to 1987-1994. Recently, *Dickson et al.* [1997] discuss increased moisture flux into the Arctic, increase ocean transport into the Arctic Ocean through the Barents Sea, and a warming and freshening of Atlantic Water inflow to the Arctic Ocean in the West Spitzbergen Current, all in connection with the increased NAO (North Atlantic Oscillation) index in the late 1980s. These pressure variations within the Arctic basin and in the North Atlantic and the North Pacific all are captured in the first empircal orthogal function (EOF) of the Northern hemisphere (>20°N) pressure field described as the Arctic Oscillation (AO) *by Thompson and Wallace* [in press]. They show in fact that the oscillation is seen throughout the arctic atmosphere up to the lower stratosphere. This lends credence to describing these oscillations fundamentally as atmospheric phenomena rather than surface or sea ice events. Below we show correlations between the winter ice flux through Fram Strait and these indices.

Our contribution to the topic is to bring to bear new data on ice motion derived from passive microwave imagery. This new source of ice motion data adds to others: buoy drift trajectories,

and tracking from higher resolution imagery such as SAR (synthetic aperture radar), Landsat, and AVHRR (Advanced Very High Resolution Radiometer). Its limitation is that fairly course spatial resolution of the imagery produces standard deviations of about 6 km for individual displacement vectors. Its great strengths are its spatial coverage and the length of the data record which is nearly twenty years for the combination of SMMR (Scanning Multifrequency Microwave Radiometer) and SSM/I (Special Sensor Microwave Imager). We use this latter asset to investigate not only the mean but also the interannual variability of flux through the strait.

In Section 2, we show monthly mean profiles of speed across our "flux gate" for eight winter months and consider the errors in area flux estimates. Section 3 presents estimates of area flux over the 18 years of SMMR and SSM/I passive microwave imagery. Our data are only for October through May; the ice is not tracked well in passive microwave imagery in summer. The estimate is extended to summer by correlating area flux with the pressure gradient across Fram Strait. In Section 4 we explore the correlation of area flux during the "deep winter" months of December through March with the index of the North Atlantic Oscillation (NAO) and with the Arctic Oscillation (AO), and show how the circulation within the Arctic Ocean varies with NAO. In Section 5 we use the ice thickness values of *Vinje et al.* [in press] to produce volume flux estimates and similarly extend them to summer by using pressure gradients across Fram Strait. Obviously our winter area flux estimates are the most robust of these estimates; our extensions to summer and volume flux are more speculative, but still useful.

2. Sea Ice Area Flux

The 37 GHz channel data from the SMMR and SSM/I instruments contain the longest satellite passive microwave record of the Arctic from 1978-present whereas the 85 GHz channel data are available for a much shorter period from 1991-present. Ice motion extracted from 37 GHz passive microwave data, albeit at lower resolution, can provide us with a multi-decadal record

for estimation of ice area flux. In this section, we demonstrate that consistent estimates of area flux can be obtained during the overlapping 37 GHz and 85 GHz datasets in the 90's. This allows us to extend the methodology, with some confidence, to the computation of ice area flux using the lower resolution channel from 1978 through 1996.

2.1 Ice Motion from Satellite Passive Microwave Data

We use ice motion from satellite passive microwave data to estimate the ice area export through Fram Strait during the winter months (October through May) of 1978-1996. The feasibility of extracting ice motion in the winter from sequential passive microwave data has been demonstrated by *Agnew et al.* [1998], *Cavalieri et al.*[1998] and *Kwok et al.* [1998]. In particular, *Kwok et al.* [1998] also demonstrated that winter ice motion can be extracted from the lower resolution 37 GHz channel of the SMMR and SSM/I radiometers in addition to the 85 GHz channel. Together, the two frequency channels provide more than eighteen years of winter ice motion from 1978-present with overlapping observations between 1991-present. Summer ice motion is unreliable due to the confounding effects of surface melt and atmospheric water vapor and estimates of summer ice area flux will not be addressed in this paper.

The ice motion used in this paper is produced by the ice tracking procedure described in *Kwok et al.* [1998]. In the motion tracker, the magnitude of the normalized cross-correlation coefficient is used as the measure of similarity between patches in the passive microwave datasets. Patches are small nxn pixel sub-images from the brightness temperature field. The method, which has been well used previously, involves finding the spatial offset that maximizes the cross-correlation coefficient of the brightness temperature fields of patches in two images separated in time. Starting with an approximate location on the second image, we compute the correlation coefficient between a patch from the first image and another patch of the same size on the second image. This correlation value is recorded. The computation is repeated at each position as the array from the first image is shifted on a two dimensional grid

to obtain an array of correlation coefficients. The peak of this sampled surface is considered to be the location of maximum; and the ice motion is the difference in geographic locations of the centers of the two patches. This procedure is repeated for each patch extracted from the first image. We focus the ice tracker on extracting ice motion from a region of approximately 780 km x 780 km centered around the flux gates shown in Fig. 1. As discussed *Kwok et al.* [1998], the ice tracker produces better quality results when the tracking procedure is applied to a subset of the brightness temperature field where the ice motion is expected to be coherent over the interval of interest.

Daily ice motion is extracted from the 85 GHz V record between 1991 and 1996. Between 1978 and 1996, 2-day ice motion is produced from the 37 GHz V passive microwave record because these brightness temperature fields are available at two-day intervals during the SMMR period (1978-1987) and a longer time separation between sequential observations increases the signal (displacement) to noise (resolution) ratio of the motion estimates. The size of the patches used in the tracking procedure are 70 km x 70 km for the 85 GHz data and 140 km x 140 km for the 37 GHz data. We sample the motion field on a uniform grid of 20 km. This creates an oversampled motion field useful in the comparison and interpolation processes discussed below.

We assess the errors associated with the measurement of ice motion near the Fram Strait by comparing contemporaneous buoy motion with the closest 85 GHz and 37 GHz ice motion sample from the gridded dataset. Table 1 shows the the difference between the winter passive microwave derived ice motion and available buoy motion which we assume to be 'truth'. For comparison, the mean displacements of the samples are shown on the same table. The mean error seems unbiased. The standard error ranges between 4.4-6.7 km for the 85 GHz channel and 7.1-13.0 km for the 37 GHz channel. The higher standard error for ice motion from the lower frequency channel is expected. In all cases, the standard errors are smaller than the mean displacement (signal) of the samples used in the comparison. We note that there is a

smaller number of samples in the 37 GHz comparison because of the 2-day motion sampling and the smaller number of observations from the 37 GHz channel.

2.2 Motion Profile across Flux Gate

We define two flux gates across the Fram Strait. Flux gate *a* is positioned along a 400 km line, roughly along 81°N, drawn across the passage between Antarctic Bay in northeast Greenland and the northwestern tip of Svalbard (Fig. 1). Flux gate *b*, positioned further south closer to where most upward-looking sonars are moored, is discussed in a later section. We placed flux gate *a* at 81°N since the area flux estimate across this line is more indicative of area export from the Arctic Ocean. Further south, ice area is typically added due to divergence of the ice cover. For the motion profile across this passage, we assume no motion at the two coastal endpoints of the flux gate. In order to avoid contamination of the motion estimates by non-ice pixels of the coast, the higher resolution 85 GHz channel can provide motion observations no closer than 35 km of the coast i.e. half the patch size used in the ice tracker.

The mean monthly 85 GHz ice motion profiles across flux gate *a* over the years 1991 through 1996 are shown in Fig. 2. To create these profiles, we first interpolate the gridded ice motion field to twenty uniformly-spaced points along the flux gate. Cubic splines, constrained to go zero at the endpoints, are then fit to the two components of the motion vectors to fill gaps in the motion estimates along the line. The vectors are projected onto the unit normal of the flux gate to obtain the magnitude of ice motion through the passage. The SMMR and SSM/I ice concentration products are used to mask out the ice free samples along the line. The east end of the passage is frequently ice free. The profiles show that the motion tend to increase rapidly and peaks at around 8-9°W, stays fairly uniform and taper off to zero around 2-3 °EWe discuss the implication of uncertainty in the shape of the motion profile near the coast later in this section.

The 37 GHz channel motion observations, however, are limited to providing observations outside of 70 km from the coast, therefore there are gaps between the observations in the center 260 km of the passage and the two coastal points. We fill in the gaps in the 37 GHz observations by using the motion profile from the 85 GHz observations with the following procedure. First, we create motion estimates at 40 km from each endpoint. We find one observation closest to the location we wish to create this motion estimate. That observation is then used to scale the average monthly 85 GHz motion profile (based on the 5-year record) to provide a motion estimate at the point. Finally, we fit cubic splines to the 37 GHz observations and the two estimates to obtain the ice motion at the twenty points along the flux line. The ice concentration masks are applied after this step.

2.3 Estimation of Area Flux - Error Analysis

We assume 100% ice concentration, within the 15% ice edge, in the calculation of the ice area flux. The area flux, F, is estimated by integrating the ice motion over the twenty points along the flux gate using the simple trapezoidal rule,

$$F = \sum_{1}^{19} 0.5(u_i + u_{i+1})\Delta x$$

where u is the magnitude of the motion perpendicular to the flux gate and Δx is the spacing between the motion estimates along the flux gate. The annual winter area flux is the sum of the daily and 2-day area flux from the beginnning of October until the end of May. Fig. 3 (and Tables 2 and 3) shows the winter area flux for the five years of overlapping 37 GHz and 85 GHz motion observations. The trend and the value of the ice flux from the two records are quite consistent during these five years (R=0.98). The average area flux over this period is 806,000 km^2 with a standand deviation of 116,000 km^2. The mean difference between the two winter flux estimates is approximately 41,000 km^2 with a standard deviation of 25,000 km^2.

First we consider the dependence of the uncertainties in the flux estimates on errors in the passive microwave ice motion. Based on the resolution of the two radiometer channels, there are 5 independent 85 GHz ice motion observations and fewer than 3 independent motion

samples from the 37 GHz observations along the flux gate. Assuming that the errors of the motion samples are additive, unbiased, uncorrelated and normally distributed, the uncertainties in the daily and 2-day area estimates, σ_F, are given by,

$$\sigma_F(km^2) = \frac{\sigma_u}{\sqrt{N_S}} L$$

where L is the length of the flux line (approximately 400 km), σ_u is the standard error in the motion estimates and N_s is the number of independent samples. For N_s =5 and σ_u =6 km, the uncertainty in the daily 85 GHz area flux is approximately 1100 km^2 compared to the average daily flux of 3300 km^2. The uncertainty is approximately 2300 km^2 (for N_s =3 and σ_u =10 km) for the 2-day 37 GHz area flux estimates compared to the average 2-day flux of 6600 km^2. On a daily basis, the estimates are rather noisy.

The uncertainty in the average winter area flux estimates, σ_T, again assuming that the errors of the area flux are additive, unbiased, uncorrelated and normally distributed is,

$$\sigma_T(km^2) = \sigma_F \sqrt{N_D}$$

where N_D is the number of observations over the winter. There are approximately 240 daily flux observations and half that many 2-day observations between October and May. This results in uncertainties in the winter area flux, σ_T, of approximately 17,000 km^2 for the daily 85 GHz observations and 25,000 km^2 for the 2-day 37 GHz observations. This amounts to less than 4% of the average annual winter area flux of about 670,000 km^2.

A second source of error in the area flux estimates is the model of the motion profile near the coast. We assume that there is no motion at the coastal endpoints of the flux gate and that the motion increases smoothly from those points to 35 km off the coast where the observations are available (Fig. 4a). A departure from this assumption would introduce biases in the area flux estimates. In the worst case, if the profile were uniform across the strait and the motion near the coasts did not go to zero (as depicted in Fig 4b), we would underestimate the area

flux by approximately 10 %. We examined ice motion derived from the ERS-1 Synthetic Aperture Radar (SAR) data within 50 km of the coastal endpoint of gate a. All 27 observations available between January and October 1993 have velocities of less than 1 km/day. These are comparable to the magnitude of ice motion in the profiles in Fig. 2. We believe that this source of error to be less than 10% and the small mean difference between the 85 GHz vs 37 GHz area flux could be introduced by the procedure used to estimate the motion samples near the coast.

Using the five years of overlapping 85 GHz and 37 GHz ice motion measurements, our procedure provided consistent estimates of area flux through the Fram Strait. We discussed the possible biases in the estimates due to the lack of knowledge of the coastal motion profiles in the data. Uncertainties in the winter ice area flux due to ice motion errors are 17,000 km^2 and 25,000 km^2 for the daily 85 GHz and 2-day 37 GHz observations. We expect the ice motion extracted from the 37 GHz channel of SMMR that had identical spatial resolution and was operational between 1978-1987 to provide us with similar error characteristics. We use the procedure described above to construct an 18-year record of winter area flux.

3. Area Flux: An 18-year record

In this section, we discuss the monthly variability, the seasonal variability and interannual variability of the flux estimates, its dependence on the gradient in the sea-level pressure across the Fram Strait and the procedure for estimating summer area flux.

3.1 Winter Area Flux

The 18-year record of winter area flux computed using the procedure described in the previous section is shown in Table 3a. Fig. 5 shows the monthly area flux from 1978-1996. The mean monthly winter flux over the entire period is 84,000 km^2. The maximum monthly winter area flux on record is 160,000 km^2 in February, 1995. Month-to-month variances are high. The

monthly mean area flux (Fig 6) shows that it typically increases starting in October to a maximum in December while staying relatively uniform from Januany to April and drops rather quickly in May.

A plot of the total winter area flux each year is shown in Fig. 7. The average winter area flux over the 18-year record (1978-1995) is 670,000 km^2, approximately 7% of the area of the Arctic Ocean. The winter area flux ranges from a minimum of 450,000 km^2 in 1984 to a maximum of 906,000 km^2 in 1995. The standard deviation in the annual winter flux is 108,000 km^2. Over the record, there seem to be an upward trend in the ice flux of approximately 9900 km^2/yr.

Here, we examine the correlation between the monthly area flux and the average monthly gradient in the sea-level pressure (SLP) across the Fram Strait over the eighteen years. Fig. 8 shows the correlation over the entire winter (October through May) and the correlation over the high flux months of December through March. Since ice motion is largely wind driven, the dependence of the area flux on the gradient in the sea-level pressure across Fram Strait is high (R = 0.85). During the months of highest area flux (December through March), the correlation is even higher - the gradient in sea-level pressure explains more than 79% of the variance (R = 0.89) in the ice area flux. Similar to the eighteen year winter flux record, there is an upward trend in the SLP gradient across the Strait. Over the record, the regression slopes are 0.13 mb/yr and 0.22 mb/yr for the winter and for the high flux months.

3.2 Summer Area Flux

To obtain year-round flux area flux estimates, we use the coefficents from the regression of the time series of area flux versus pressure gradient across the Fram Strait. The monthly summer area flux, F_{summer}, shown in Table 3b is estimated using the following relationship,

$$F_{summer} = 8394\Delta P + 61218 \quad (km^2)$$

where ΔP (mbar) is the mean monthly pressure gradient across the Fram Strait. The time-series of ice flux during the summer months is shown in Fig. 5. The residual of the regression analysis is 7400 km^2 or 12% of the average monthly area flux. Including the summer area flux, the average annual ice area flux is 919,000 km^2 over the 18-year record. The summer months contribute approximately 27% of the ice area to the annual area exported through the Fram Strait.

4. Winter Area Flux and NAO

We find a strong connection between the winter area flux and the North Atlantic Oscillation (NAO). The NAO is a major source of interannunal variability in the atmospheric circulation pattern in the North Atlantic [*Hurrell*, 1995] and is most pronounced during winter and accounts for more than one-third of the total variance in the sea-level pressure (SLP). *Hurrell* [1995] defined an index of the NAO as the SLP anomalies between Lisbon, Portugal and Stykkisholmur, Iceland. The positive phase of NAO is characterized by an intense Icelandic low with a strong Azores ridge to its south. This low affects to a broad region of anomalously low pressure in the Arctic. The signs of these anomalies are reversed during the negative phase of the index.

Since the atmospheric pattern due to NAO is most pronounced during winter, we compare the time series of total DJFM (December through March) ice area flux and the average DJFM NAO index over the 18-year record in Fig. 9. The correlation is quite remarkable. High (Low) area flux is associated with positive (negative) extremes of the NAO index. The scatterplot shows a correlation of R=0.66 between the DJFM ice area flux and the DJFM NAO index. We note that the one data point that seems to be an outlier is associated with the low index year (NAO < -2) of 1995. Excluding this data point from the regression, we obtain an R=0.86. The DJFM index explains 72% of the variance of the winter area ice when NAO>-1. We raise two obvious questions here: 1) How does the NAO affect the flux of sea ice through Fram Strait?; 2) Why do

years of high NAO index explain a larger percentage of the variance in the winter ice area export?

NAO and Sea-level Pressure

Since ice motion is largely wind-driven and is nearly parallel to isobars of surface pressure, we examine the difference (Fig. 10) between the average SLP over the polar regions for the months of December through March (1978-1996) when the average monthly NAO index > +1 and when the NAO index <-1. Sea-level pressure fields were provided by the International Arctic Buoy Program (IABP). Of the 72 winter months of December through March between 1978 and 1996, there were 38 months with NAO>+1 and 22 months with NAO<-1. When the NAO index is greater than one, the SLP gradient across the Fram Strait is high as evidenced by the increased density of isobars around the east coast of Greenland. The time series of monthly averaged (DJFM) gradient in the SLP across Fram Strait and the NAO index is high correlated (Fig. 11). Positive NAO produces higher winds through the Fram Strait thus enhancing ice area export. We also note that the enhanced wind forcing is equally pronounced over the Denmark Strait. The difference field (Fig. 11c) shows a large-scale depression of more than 12 mb centered east of Iceland that affects a broad region of the Arctic and extends all the way to the Bering Strait when the NAO is positive. The pressure contours are positioned in such a manner as to increase the SLP gradient (approximately 1 mbar) around the east coast of Greenland. The negative pressure contours show lower than average SLP over the entire Arctic during the NAO>+1 months. Correlation between the area flux and NAO index is reduced during months with negative NAO indices because of decreased dominance of the large-scale Icelandic low on the sea-level pressure gradient across the Fram Strait. Over the 18-year period, there is a correspondence between the upward trend in the winter ice area flux and the winter NAO index.

Walsh et al. [1996] reported a decrease in the annual mean SLP in the second half of the period 1979-1994. We believe that this decrease in SLP in the Arctic is strongly linked to the intensity of the Icelandic Low as measured by the NAO index. The Arctic scale influence of the Icelandic

Low can be seen in Fig. 11. In recent years, a sustained positive phase of the NAO index is associated with lower than average SLP in the Arctic. The negative phase of NAO dominated the circulation from the mid-1950's through the winter of 1978/79. This is followed by a transition to recurring positive phases of the NAO during the winter of 1979/80, with the atmosphere remaining locked in this mode through the winter season of 1994/95. Except for the rather dramatic reversal in phase of the NAO in the winter of 1995/96, the mean annual NAO indices were strongly positive in the late 80's and early 90's. The mean annual NAO indices are 0.15 and 0.45 for the years 1979-1986 and 1987-1994. It is not surprising that a lower SLP is observed in the second half of the period 1979-1994 since high NAO indices are associated with lower SLP. Table 4 summarizes the correlation of the four DJFM time-series of area flux, NAO index, ΔP and P. ΔP is the gradient in SLP across Fram Strait and P is the average SLP over the Fram Strait. The correlations between the time-series of area flux, NAO index and ΔP are significant and positive, whereas the correlations between P and the above three quantities are negative, although not as strong. A decrease (increase) in P is generally associated with an increase (decrease) in area flux, NAO index and ΔP. The recent decrease in SLP can be partially explained by the positive phases of NAO since 1988.

NAO, Arctic Oscillation (AO) and Ice flux

Recently, *Thompson and Wallace* [1998] described an Arctic Oscillation (AO) pattern and associated index obtained from the analysis wintertime SLP record (1958-1997) poleward of 20°N using empirical orthogonal functions. The AO pattern, covering a larger horizontal scale and incorporates many of the features of the NAO, has a mode of the oscillation that involves a seesaw of SLP between the Arctic basin and the surrounding zonal ring. We find a correlation of 0.73 between the DJFM NAO and AO indices from 1978-1996. Over the same 18-year period, the correlation between the DJFM AO indices and ice area flux through Fram Strait is 0.64. In fact, *Thompson and Wallace* [1998] also showed that the AO pattern and the 50 mbar height patterns are strongly correlated demonstrating vertical coupling between the lower

atmosphere and the strength of polar vortex. This lends credence to describing these oscillations fundamentally as atmospheric phenomena rather than surface or sea ice events. They exert significant influence on the ice balance of the Arctic Ocean.

5. Volume Flux: 1990-1995

To compute the ice volume flux, we use the cross-strait thickness profile at 79°N (gate *b* in Fig. 1) as parameterized by *Vinje et al.* [1998]. The ice thickness, h, as a function of longitude, λ, is given by,

$$h(\lambda,t) = \begin{cases} h_o(t)(-0.127\lambda + 0.37) & 0^o < \lambda < 2.9^o \\ 0.68h_o(t) & -5^o < \lambda < 0^o \\ h_o(t) & \lambda \le -5^o \end{cases}$$

where $h_o(t)$ is the thickness at 5°W. This thickness profile is derived from upward-looking sonar (ULS) observations at different locations and times in 1992, 1993 and 1995. The monthly mean h_o, between October 1990 and July 1996 from ULS measurements are given in Table 9 of *Vinje et al.* [1998].

Using this thickness profile estimate, the monthly volume flux, F_v, is,

$$F_v(t) = \int_{coast}^{iceedge} h(x,t)u(x,t)\,dx$$

where x is the distance along the flux gate and $u(x,t)$ is the motion profile at 79°N. We derive another set of motion profiles along 79°N from our gridded ice motion observations using the procedures described in section 2. The uncertainty in the volume flux, σ_V, can be estimated by,

$$\sigma_V = \sqrt{(A\sigma_h)^2 + (h\sigma_T)^2}$$

where A is the area flux, h is the ice thickness and σ_h is the error in the thickness estimates. *Vinje et al.* [1998] assumes an error of 0.1 m for σ_h. Using typical numbers for A, h and σ_T (670,000 km^2, 3 m, and 25,000 km^2, respectively) gives an uncertainty in the volume flux of approximately 100 km^3 which is less than 6% of the 5-year average winter volume flux. Again,

errors in our assumption of the shape of the motion profile (discussed in Section 2) near the coast would lead to a worst case underestimation of the winter volume flux by 240 km^3 or 14%.

The computed winter volume flux for 1990-1995 are shown in Table 5a. The correlation between the winter volume flux and area flux shown in Fig. 13 is 0.93. The interannual variability is high. The average volume flux over the six years is 1745 km^3 ranging over more than a factor of 2 from a low of 1375 km^3 in 1990 to a high of 2791 km^3 in 1994. Regression of the DJFM NAO index and volume flux time-series between 1990-1995 gives a correlation of 0.56. This strong correlation between the NAO and the volume flux was also reported by Dickson et al. [1998].

We can crudely extrapolate our winter estimate through summer to obtain a mean annual estimate. If simply we multiply our 8-month value by 1.5 to allow for four summer months, we obtain a mean flux of 2617 km^3/yr. However, it appears that summer fluxes are lower than winter fluxes. From Table 10 of Vinje et al. [1998], one computes a winter volume flux that is 78% of the total. If we use that figure to scale our winter value, we obtain a mean annual volume flux of 1745/0.78 or 2237 km^3/yr.

Another approach to compute the summer volume flux is to first estimate the monthly motion profiles at gate *b*. We use the summer area flux (estimated using the procedure discussed in Section 3) to weigh an area-normalized May motion profile, $\tilde{u}(x)$, across gate *b* to obtain an estimated motion profile,

$$u(x,t) = A_{summer}(\Delta P,t)\tilde{u}(x,t).$$

The volume flux, F_V, is then computed using the thickness data as described above. Table 5b shows these summer volume flux estimates. The time-series of these estimates are plotted in Fig. 12. The mean annual area flux over the period 1990-1995 is 2366 km^3, with the summer contributing approximately 24% to the total volume. This is our best estimate of the mean volume flux.

In Table 5b, we compare our volume flux with the estimates of *Vinje et al.* [1998]. The primary difference between our procedures is that their ice flux is estimated using a parameterization of the ice motion based on the pressure gradient across the Fram Strait while ours is based on ice motion derived from satellite passive microwave data. The trend is similar but lower by approximately 650 km^3. Table 6 shows other volume flux estimates as much as two times greater although results from recent work are more comparable. A lower value by Thomas et al. [1996] covers a period of low NAO. Certainly, given the range of variability of ice flux in our six-years record and potential decadal trends in this quantity, care should be taken in comparing non-contemporaneous ice flux records.

6. Conclusions

We have constructed an 18-year record (1978-1996) of ice area flux and a shorter record of volume flux (1990-1995) through the Fram Strait using records of ice motion fields derived from satellite passive microwave imagery, surface pressure fields and measured ice thickness.

We summarize the results:

1. The average winter (October through May) area flux over the 18-year record (1978-1996) is 670,000 km^2. The winter area flux ranges from a minimum of 450,000 km^2 in 1984 to a maximum of 906,000 km^2 in 1995. We observe an upward trend in the winter flux of approximately 9900 km^2/yr. The average summer (June through September) area flux is 249,000 km^2 giving a mean annual area flux of 919,000 km^2, approximately 9% of the Arctic Ocean.
2. The average winter (October through May) volume flux over the six years (1990-1995) is 1745 km^3 ranging from a low of 1375 km^3 in 1990 to a high of 2791 km^3 in 1994. The average summer (June through September) volume flux over the same period is 559 km^3. The mean 8-month winter volume flux contributes more than 76% of the total annual flux of 2366 km^3.

3. Over the 18-year record, the gradient in the sea-level pressure across the Fram Strait explains more than 72% of the variance in the winter area flux.
4. The NAO index (>1) explains almost 74% of the variance of the winter area flux. Correlation is reduced if we include the low NAO index winter of 1995/96 because the decreased dominance of Icelandic Low in the spatial distribution of sea-level pressure. The upward trend in the area flux is reflected in the upward trend in the winter NAO index over the 18-year record. There is a large reversal in the NAO index in 1996 to its lowest level after almost two decades of upward trend. It is not clear how the Arctic and ice export will be affected by this dramatic change in the NAO. Over our six-year record of volume flux estimates, the correlation between the DJFM NAO index and the volume flux is 0.56.
5. The recent decrease in sea-level pressure in the central Arctic [*Walsh et al.*, 1996] is linked to the sustained positive phase of the NAO during the late 80's and early 90's when the intense Icelandic Low decreases the mean sea-level pressure of not just the subpolar oceans in the Eurasian sector, but over a broad region of the central Arctic. We observe significant positive correlations between the time-series of area flux, gradient in the sea-level pressure across the Fram Strait and the NAO index. All three exhibit positive trends during this period. The record of absolute sea-level pressure at the Fram Strait is, however, negatively correlated to these three time-series indicating a decreasing trend in sea-level pressure.

Acknowledgment

The SSM/I data were provided by World Data Center A for Glaciology/National Snow and Ice Data Center, University of Colorado, Boulder, CO. We wish to thank A. Schweiger for providing the ERS-1 SAR ice motion dataset over the Fram Strait and S. Pang for providing software support during this study. R. Kwok performed this work at the Jet Propulsion Laboratory, California Institute of Technology, sponsored by the National Oceanic and Atmospheric Administration and the National Aeronautics and Space Administration. D. A. Rothrock performed this work at the Applied Physics Laboratory, University of Washington as part of 'Polar Exchangeat the Sea Surface (POLES)' under NASA contract, NAGW-2407.

References

Aagaard, K., and E. Carmack, The role of sea ice and other fresh water in the Arctic circulation, *J. Geophys. Res. 94*(C10), 14,485-14,498, 1989.

Dickson, R.R., J. Meincke, S.-A. Malmberg, and A.J. Lee, The "great salinity anomaly" in the northern North Atlantic 1968-1982, *Progr. Oceanogr., 20*, 103-151, 1988.

Dickson, R. R., T. J. Osborn, J. W. Hurrell, J. Meincke, J. Blindheim, B. Adlandsvik, T. Vinje, G. Alekseev, W. Maslowski and H. Cattle, The Arctic Ocean response to the North Atlantic Oscillation, in Proceedings of the Polar Processes and Global Climate Conference, Orcas Island, 40-41, 1997.

Hurrell, J. W. Decadal trends in the North Atlantic Oscillation: regional temperatures and precipitation, *Science*, 269, 676-679, 1995.

Kwok, R., A. Schweiger, D. A. Rothrock, S. Pang and C. Kottmeier, Sea ice motion from satellite passive micrwave data assessed with ERS and buoy motions, *J. Geophy. Res.*, 103(C4), 8191-8214, 1998.

Martin, T., Sea ice drift in the East Greenland Current, *Proc. 4th Symp. Rem.Sens. Polar Envir.*, Lyngby, Denmark, 29 April - 1 May 1996, ESA SP-391, July 1996.

Moritz, R. *The Ice Budget of the Greenland Sea*, Ph.D. Thesis, Yale University, 1988 .

Proshutinsky, A. Y. and M. A. Johnson, Two circulation regimes of the wind-driven Arctic Ocean, *J. Geophy. Res.*, 102, 12,493-12,514, 1997.

Serreze, M.C., J.A. Maslanik, R.G. Barry, and T.L. Demaria, Winter atmospheric circulation in the Arctic Basin and possible relationships to the Great Salinity Anomaly in the Northern North Atlantic, *Geophys. Res. Let., 19*(3), 293-296, 1992.

Steele, M., D. Thomas, D. Rothrock, S. Martin, A simple model study of the Arctic Ocean Fresheater balance 1979-1985, *J. Geophys. Res. 101*(C9), 20,833-20,848, 1996.

Thomas, D., S. Martin, D. Rothrock and M. Steele, Assimilating satellite concentration data into an Arctic sea ice mass balance model, 1979-1985, 101(C9), 20,849-20,869, 1996.

Thompson, D. W. J. and J. M. Wallace, The arctic oscillation signature in the wintertime geopotential height and temperature grids, *Geophys. Res. Lett.*, in press.

Vinje, T. and O. Finnekasa, The ice transport through the Fram Strait, *Norsk Polarinstitutt Report*, 186, 39pp., 1986.

Vinje, T., N. Norland and A. Kvambekk, Monitoring ice thickness in Fram Strait, *J. Geophy. Res.*, in press.

Wadhams, P., Sea ice thickness distribution in Fram Strait, *Nature*, 305, 108-111, 1983.

Walsh, J. E., W. L . Chapman and T. L. Shy, Recent decrease of sea-level pressure in the Central Arctic, *J. of Clim.*, 9, 480-486, 1996.

Figure Captions

Figure 1. (a) Location of flux gates *a* and *b* in the Fram Strait. (b) A sample ice motion field derived from 85 GHz passive microwave observations.

Figure 2. Averaged monthly (1991-1995) ice motion profiles across flux gate *a*. (a) October, (b) November, (c) December, (d) January, (e) February, (f) March, (g) April, (h) May.

Figure 3. Comparsion of time-series of winter (October through May) area flux estimates from 1-day 85 GHz and 2-day 37 GHz ice motion, 1991-1995.

Figure 4. Normalized motion profile across flux gate (a) illustration of profile with no motion at the coastal boundaries, and (b) potential worst case scenario when motion does not go to zero.

Figure 5. Time-series of monthly area flux from 37 GHz ice motion at gate *a*, 1978-1996.

Figure 6. Mean monthly area flux, 1978-1996.

Figure 7. Time-series of total area flux at gate *a* over the winter (October through May) and summer months (June through September), 1978-1996.

Figure 8. Time-series and scatterogram showing the correlation between monthly area flux and gradient in the monthly sea-level pressure across the Fram Strait. (a) October through May; (b) December through March.

Figure 9. (a) Time-series and (b) scatterogram showing the correlation between winter (December through March) area flux and NAO index, and (c) regression fit after excluding the low NAO index year of 1995.

Figure 10. Mean sea-level pressure for the months of December through March (1978-1996). (a) NAO index > +1, (b) NAO index <-1, (c) difference between (a) and (b). (Contour interval: 1mbar)

Figure 11. (a) Time-series and (b) scatterogram showing the correlation between gradient in the mean monthly sea-level pressure across the Fram Strait and the NAO index.

Figure 12. Time-series of volume flux at gate *b*, 1990-1995.

Table 1

Error Analysis - Difference between Passive Microwave Ice Motion with Buoy Motion (km)

Year	2-day 37V				1-day 85V			
	Mean	S.D.	#Obs	ean Motion	Mean	S.D.	#Obs	Mean Motion
87-88	0	6.1	21	16.6				
88-89	0.5	10	101	20.5				
89-90	-3.4	8	25	22.8				
90-91								
91-92	-0.1	13	29	20.1	0.9	6.7	115	9.3
92-93	0.4	11.2	49	17.5	0.2	5.9	251	9.9
93-94	-1.9	7.1	56	21.7	0.9	4.4	261	9.8
94-95	0.6	9.8	56	27.2	-0.2	6.4	228	15
95-96	-0.8	7.4	15	23.1	0.3	6.6	102	12.3

Table 2

Winter (October through May) Area Flux Through Fram Strait
from 1-day 85 GHz Ice Motion (km2) and difference between
Area Flux from 85 GHz and 37 GHz (from Table 3)
1991-1995

Year	Oct	Nov	Dec	Jan	Feb	Mar	Apr	May	Total	Mean	S.D.	Area Flux
91-92	98	97	116	108	101	131	58	89	798	100	21	24
92-93	76	58	121	131	127	111	102	76	803	100	27	16
93-94	84	2	155	152	65	156	119	48	781	98	57	50
94-95	138	87	156	137	158	136	132	43	987	123	39	81
95-96	66	74	108	89	95	75	82	74	663	83	14	32
Avg	92	63	131	124	109	122	99	66	806			
S.D.	28	37	23	25	35	31	29	20	116			

Table 3a
Winter (October through May) Area Flux Through Fram Strait
from 2-day 37 GHz Ice Motion (km^2)
1978-1995

Year	Oct	Nov	Dec	Jan	Feb	Mar	Apr	May	Total	Avg	S.D.
78-79	76	98	56	73	72	66	73	91	605	76	13
79-80	23	103	123	71	75	47	57	17	516	64	37
80-81	102	83	138	136	74	78	85	66	762	95	28
81-82	43	92	104	93	101	95	95	37	661	83	27
82-83	-8	74	119	160	87	84	90	25	630	79	52
83-84	88	107	102	62	116	86	70	20	650	81	31
84-85	38	53	-21	73	92	75	85	57	452	57	36
85-86	95	99	109	79	73	93	74	64	686	86	15
86-87	120	100	44	30	93	77	82	21	566	71	35
87-88	66	94	83	60	63	105	129	67	666	83	24
88-89	59	105	112	108	106	115	96	52	755	94	25
89-90	110	71	104	52	122	106	63	60	689	86	27
90-91	78	75	123	91	37	53	78	51	587	73	27
91-92	98	97	116	108	97	104	88	66	774	97	15
92-93	78	86	106	127	129	95	90	75	787	98	21
93-94	86	51	90	128	70	143	115	47	731	91	35
94-95	128	99	128	129	160	120	117	26	906	113	39
95-96	44	62	110	93	92	85	89	55	632	79	23
Avg	73	86	97	93	92	90	87	50	670	84	
S. D.	35	18	38	34	28	24	19	21	108	13	

Table 3b
Annual ice area flux. Summer area flux computed using
pressure gradient across Fram Strait

Year	Oct-May*	Jun	Jul	Aug	Sep	Total
78-79	605	57	48	55	97	863
79-80	516	65	60	58	64	762
80-81	762	99	53	26	64	1004
81-82	661	86	61	58	67	933
82-83	630	64	60	83	85	922
83-84	650	75	54	41	68	889
84-85	452	68	43	66	91	719
85-86	686	57	53	49	93	937
86-87	566	59	75	66	66	831
87-88	666	57	66	40	78	906
88-89	755	57	54	71	79	1016
89-90	689	59	40	65	56	910
90-91	587	54	62	58	81	843
91-92	774	65	54	46	52	990
92-93	787	59	56	32	64	997
93-94	731	64	51	59	62	968
94-95	906	56	90	75	84	1211
95-96	632	43	42	53	64	834
Avg	670	64	57	56	73	919

Note: Oct-May area flux from Table 3a

Table 4

Correlation between the time-series of winter (October through May, 78-95) area Flux, NAO index, gradient in sea level pressure across Fram Strait and average sea level pressure near Fram Strait

(a) Correlation (Oct-May, 1978-1995)

	Flux	*NAO*	*Δ P*	*P*
Flux	1.00			
NAO	0.28	1.00		
Δ P	0.85	0.28	1.00	
P	-0.36	-0.16	-0.25	1.00

(b) Correlation (Dec-Mar, 1978-1995)

	Flux	*NAO*	*Δ P*	*P*
Flux	1.00			
NAO	0.66	1.00		
Δ P	0.89	0.70	1.00	
P	-0.32	-0.21	-0.29	1.00

(c) Correlation - (Dec-Mar) excluding winter of 1995-1996

	Flux	*NAO*	*Δ P*	*P*
Flux	1.00			
NAO	0.86	1.00		
Δ P	0.90	0.82	1.00	
P	-0.32	-0.18	-0.28	1.00

Table 5a
Winter (October through May) ice volume flux (km^3)
from ice motion and ice thickness data
1990-1995

Year	Oct	Nov	Dec	Jan	Feb	Mar	Apr	May	Total (km^3)
90-91	172	172	291	191	173	172	149	55	1375
91-92	146	157	209	261	238	309	94	244	1659
92-93	123	123	196	206	192	267	153	117	1377
93-94	136	12	324	344	149	411	326	126	1828
94-95	327	267	457	354	319	453	462	152	2791
95-96	145	109	198	206	138	218	240	188	1441
Mean	175	140	279	261	202	305	237	147	1745

Table 5b
Annual ice volume flux (km^3). Summer volume flux estimated
using pressure gradient across gate b and ice thickness (see text)

Year	Oct-May*	Jun	Jul	Aug	Sep	Total (km^3)	Vinje et al. [1998]
90-91	1375	200	128	45	57	1805	2182
91-92	1659	228	245	147	124	2404	2848
92-93	1377	217	175	61	93	1922	2368
93-94	1828	140	112	103	157	2340	3077
94-95	2791	137	145	144	141	3358	4606
Mean		184	161	100	114	2366	3016

*Oct-May volume flux from Table 5a

Table 6
Comparison of Annual Volume Flux Estimates

Publication	Period	Location	Volume Flux ($km^3\ yr^{-1}$)
Wadhams [1983]	76	79N-81N	4000
Vinje and Finneskasa [1986]	76-84	81N	5000
Thomas et al. [1996]	79-85	81N	1900
Vinje et al. [1998]	90-96	79N	2843
Kwok and Rothrock [this paper]	90-95	79N	2366

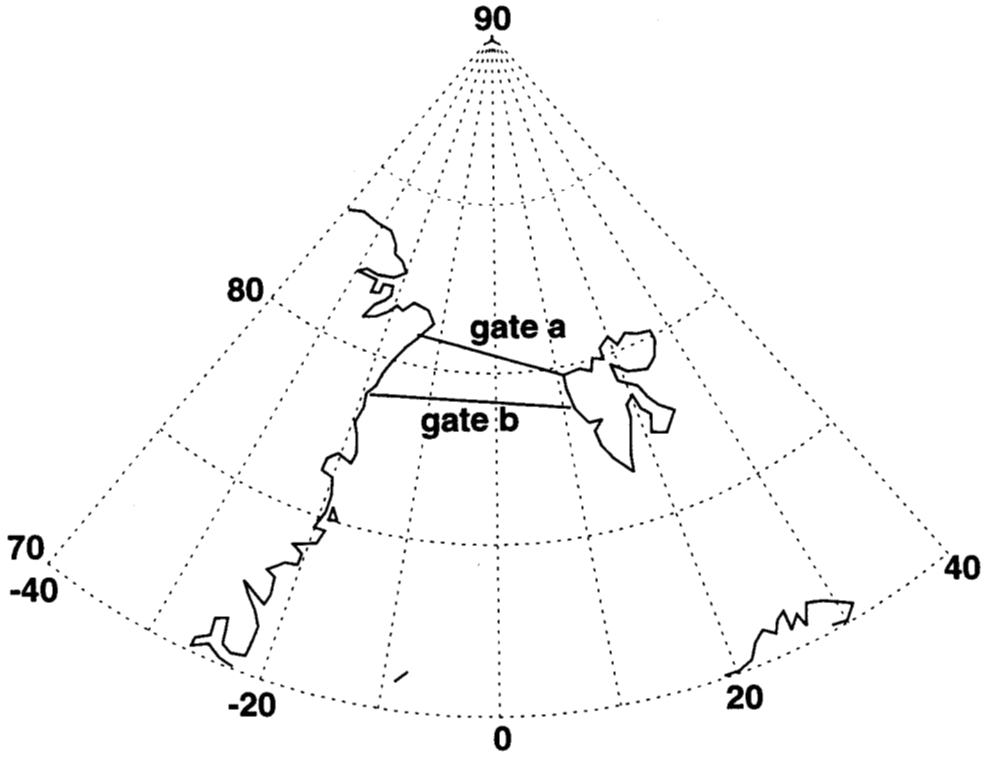
90
80
gate a
gate b
70
-40
40
-20
20
0

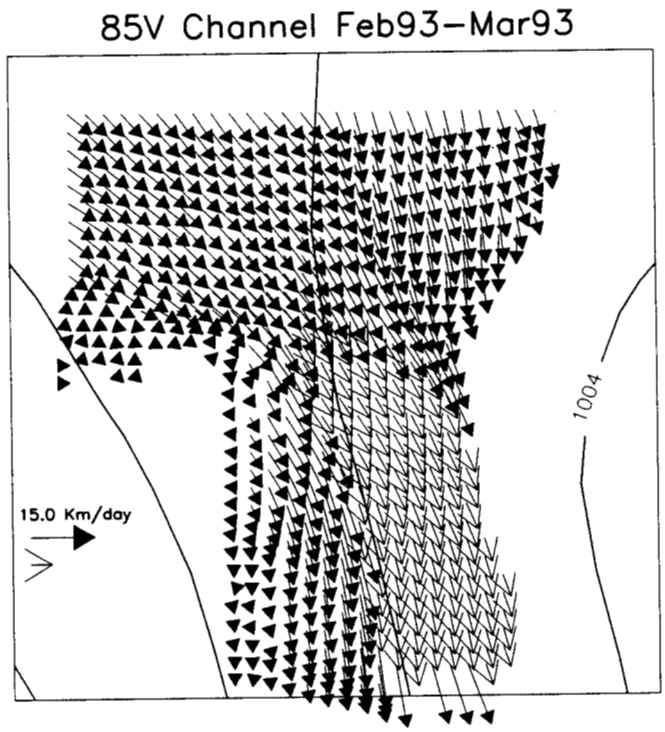
85V Channel Feb93–Mar93
1004
15.0 Km/day

Fig. 1

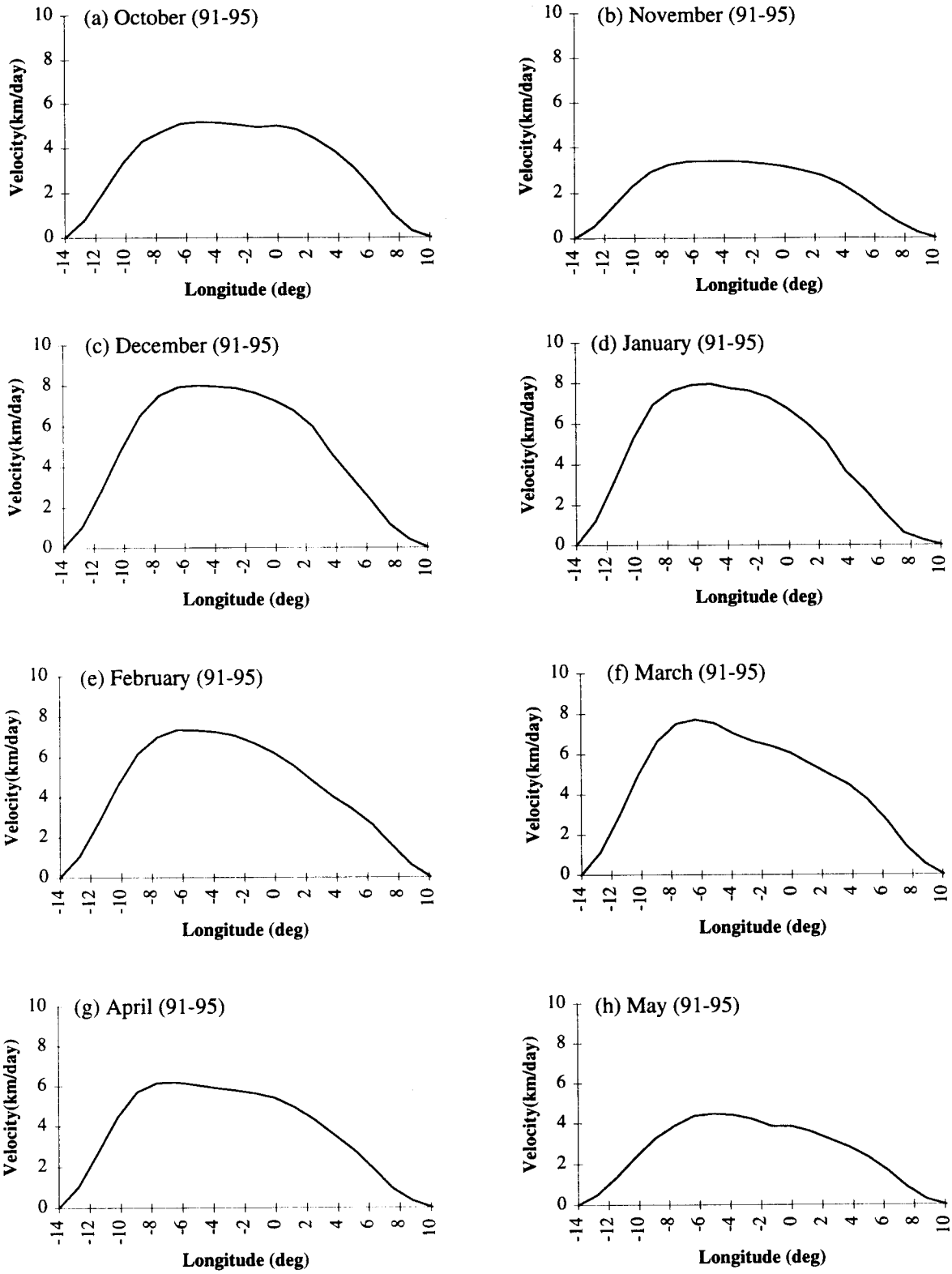
(a) October (91-95)
(b) November (91-95)
(c) December (91-95)
(d) January (91-95)
(e) February (91-95)
(f) March (91-95)
(g) April (91-95)
(h) May (91-95)
Velocity(km/day)
Longitude (deg)
10
8
6
4
2
0
-14
-12
-10
-8
-6
-4
-2
0
2
4
6
8
10

Fig. 2

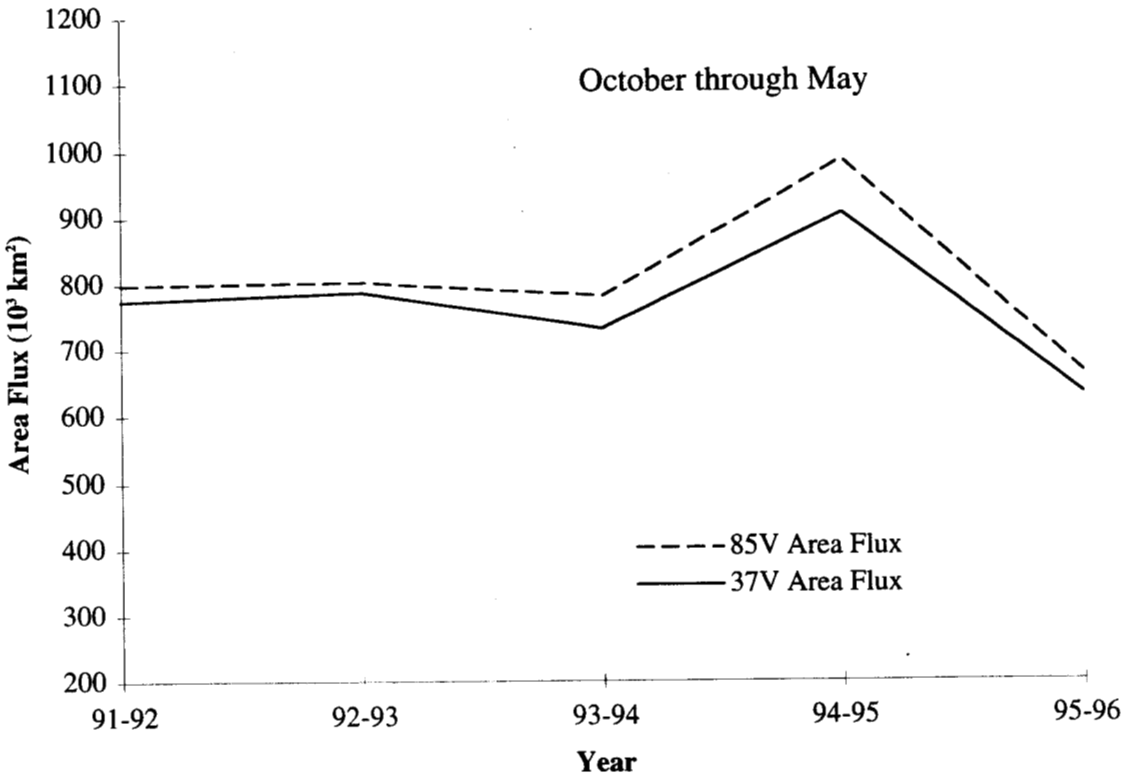
October through May
Area Flux (10^3 km^2)
1200
1100
1000
900
800
700
600
500
400
300
200
91-92
92-93
93-94
94-95
95-96
Year
85V Area Flux
37V Area Flux

Fig. 3

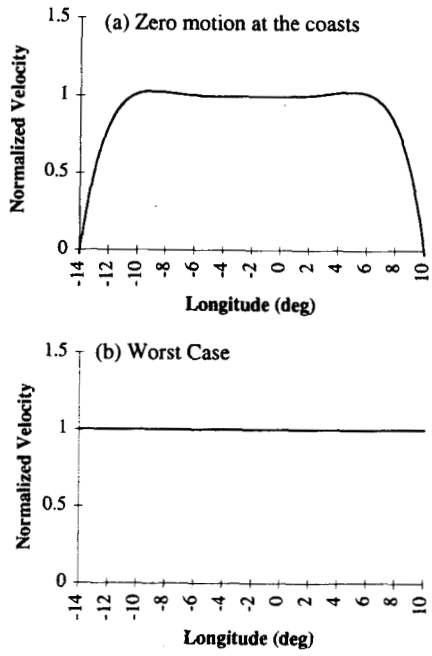
(a) Zero motion at the coasts
Normalized Velocity
1.5
1
0.5
0
-14
-12
-10
-8
-6
-4
-2
0
2
4
6
8
10
Longitude (deg)
(b) Worst Case
Normalized Velocity
1.5
1
0.5
0
-14
-12
-10
-8
-6
-4
-2
0
2
4
6
8
10
Longitude (deg)

Fig . 4

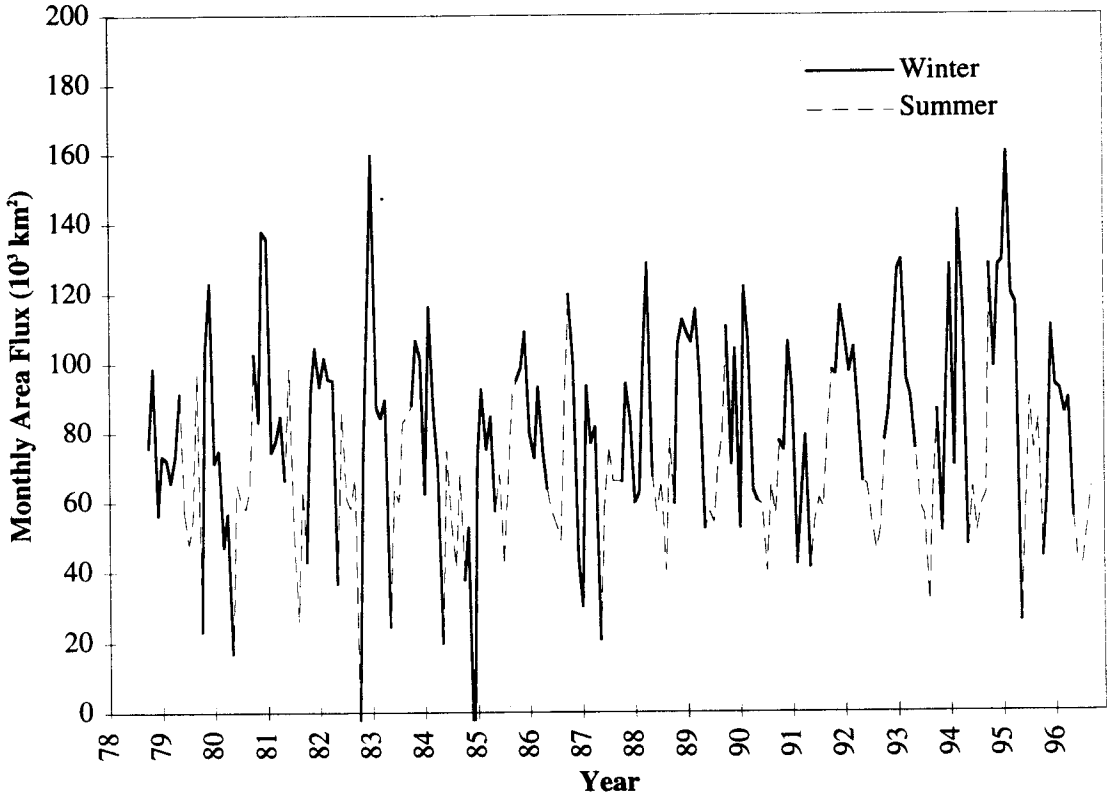
Winter
Summer
Monthly Area Flux (10^3 km^2)
200
180
160
140
120
100
80
60
40
20
0
78
79
80
81
82
83
84
85
86
87
88
89
90
91
92
93
94
95
96
Year

Fig. 5

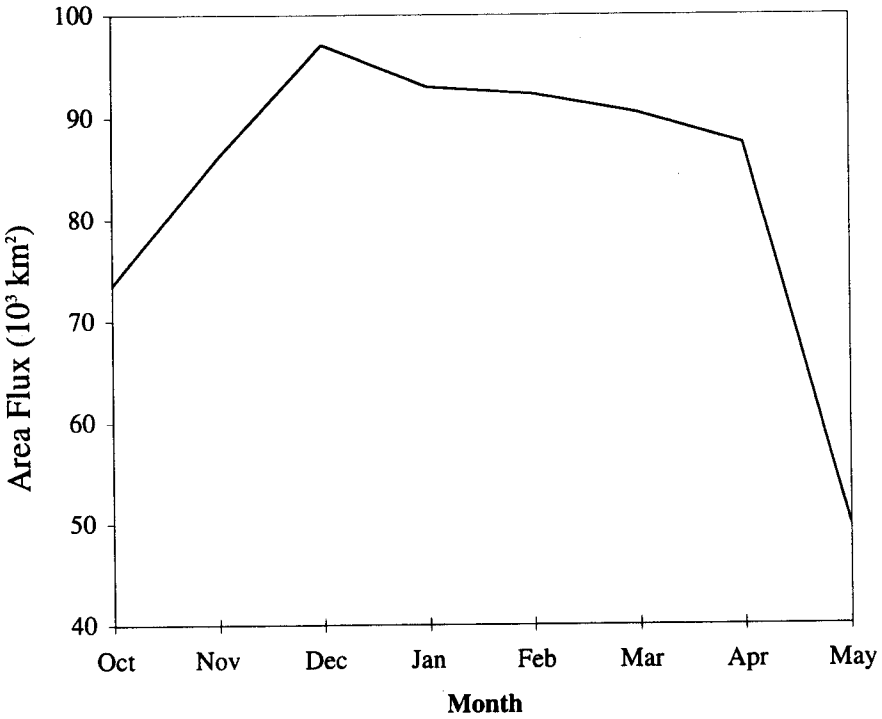
100
90
80
70
60
50
40
Area Flux (10^3 km^2)
Oct
Nov
Dec
Jan
Feb
Mar
Apr
May
Month

Fig. 6

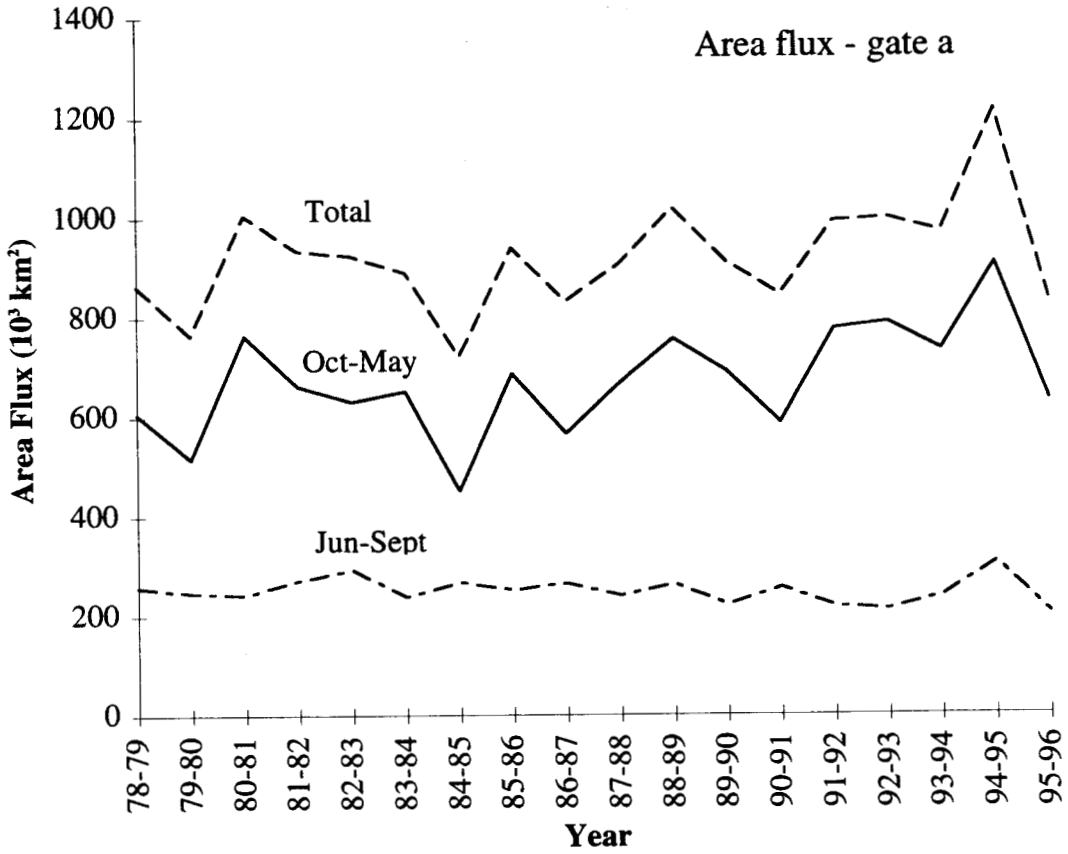
Area flux - gate a
Total
Oct-May
Jun-Sept
Area Flux (10^3 km^2)
1400
1200
1000
800
600
400
200
0
78-79
79-80
80-81
81-82
82-83
83-84
84-85
85-86
86-87
87-88
88-89
89-90
90-91
91-92
92-93
93-94
94-95
95-96
Year

Fig. 7

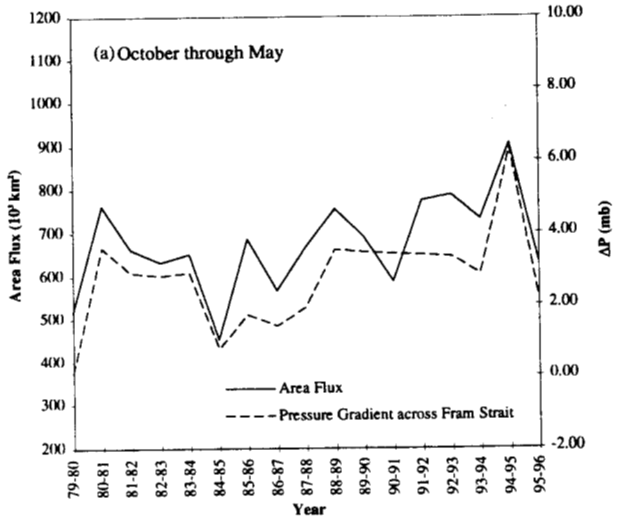
(a) October through May
Area Flux (10³ km²)
ΔP (mb)
Year
Area Flux
Pressure Gradient across Fram Strait

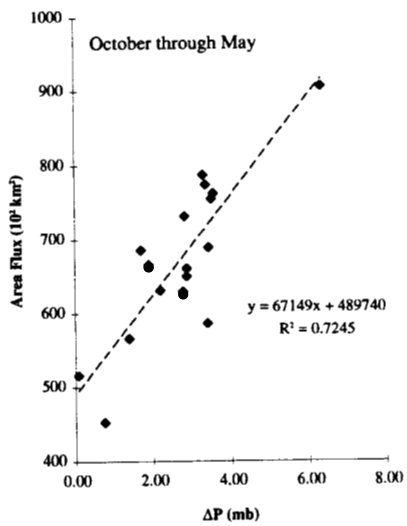
October through May
Area Flux (10³ km²)
ΔP (mb)
y = 67149x + 489740
R² = 0.7245

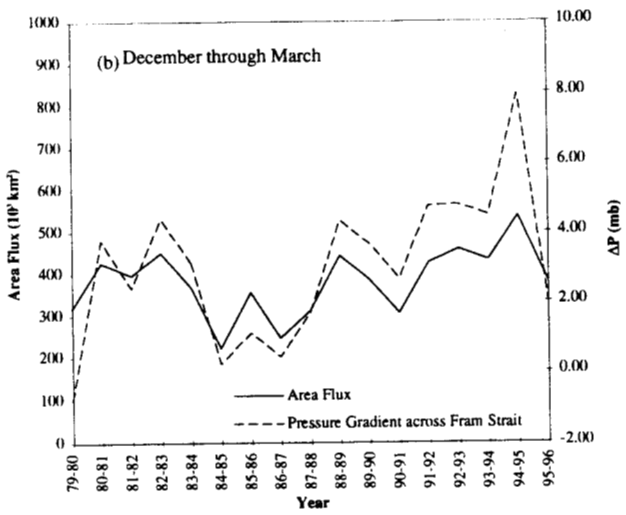
(b) December through March
Area Flux (10³ km²)
ΔP (mb)
Year
Area Flux
Pressure Gradient across Fram Strait

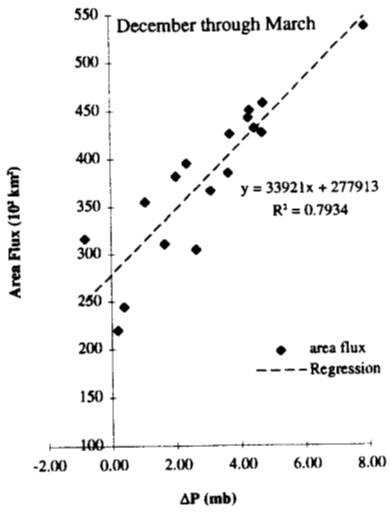
December through March
Area Flux (10³ km²)
ΔP (mb)
y = 33921x + 277913
R² = 0.7934
area flux
Regression

Fig. 8

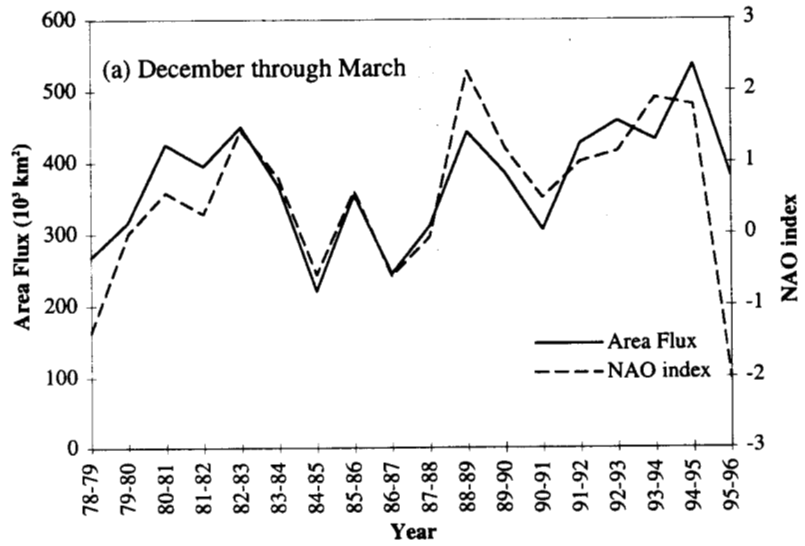
(a) December through March
Area Flux (10³ km²)
NAO index
Year
Area Flux
NAO index
600
500
400
300
200
100
0
3
2
1
0
-1
-2
-3
78-79
79-80
80-81
81-82
82-83
83-84
84-85
85-86
86-87
87-88
88-89
89-90
90-91
91-92
92-93
93-94
94-95
95-96

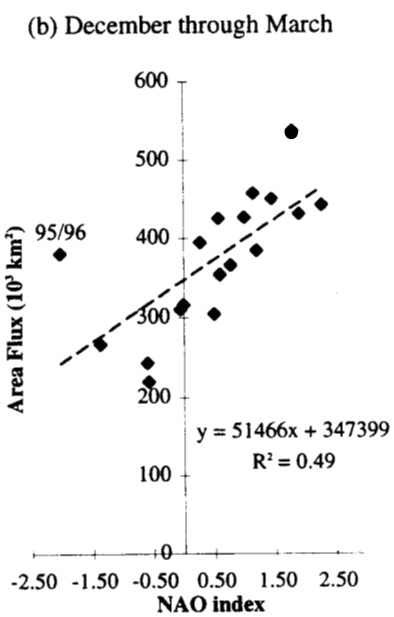
(b) December through March
Area Flux (10³ km²)
NAO index
95/96
y = 51466x + 347399
R² = 0.49
600
500
400
300
200
100
0
-2.50
-1.50
-0.50
0.50
1.50
2.50

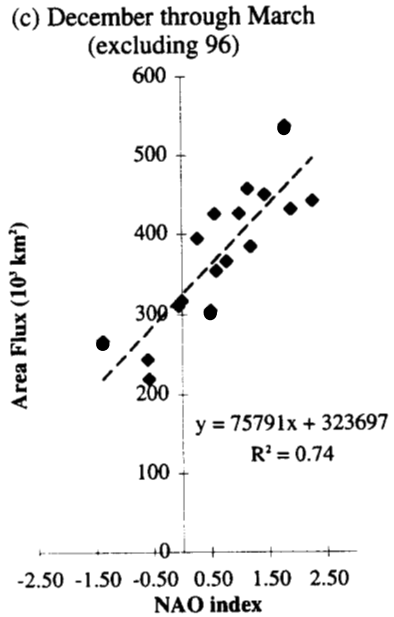
(c) December through March
(excluding 96)
Area Flux (10³ km²)
NAO index
y = 75791x + 323697
R² = 0.74
600
500
400
300
200
100
0
-2.50
-1.50
-0.50
0.50
1.50
2.50

Fig. 9

(a)

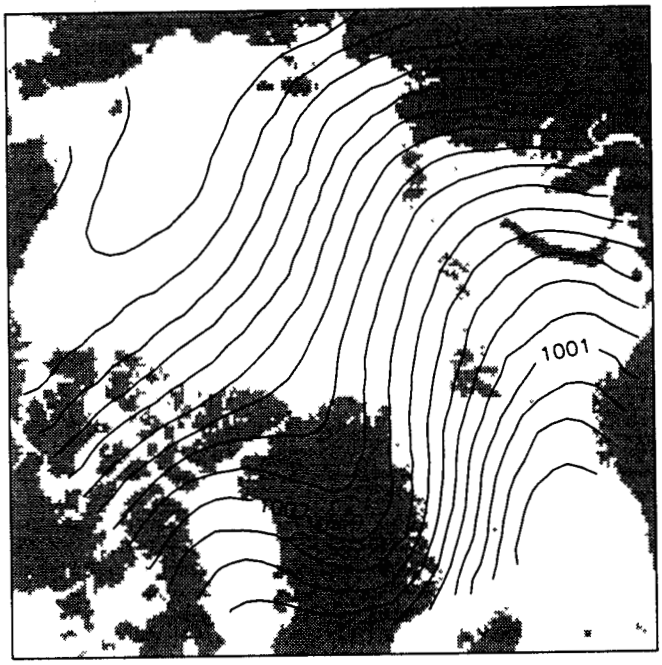

(b)

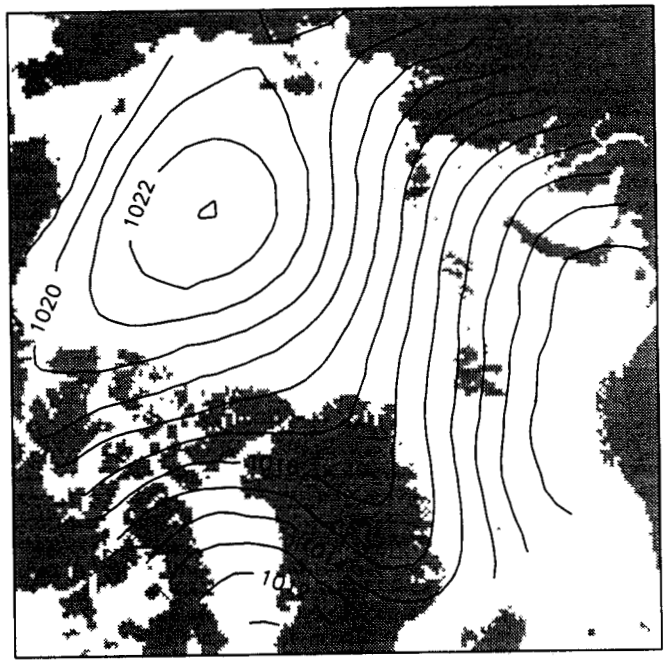

(c)

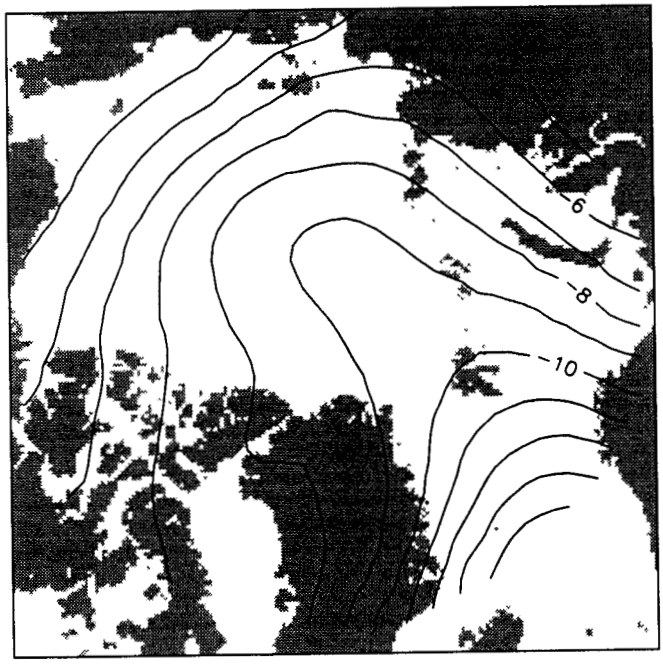

Fig. 10

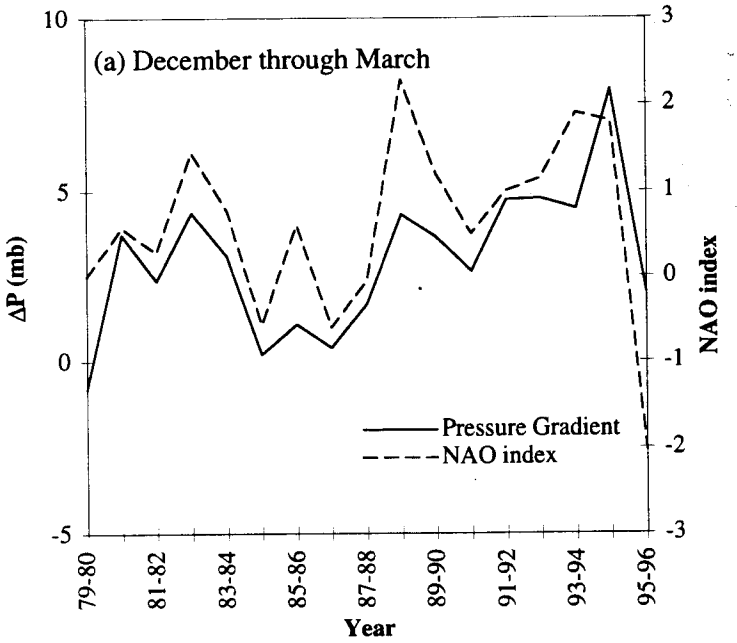
(a) December through March
ΔP (mb)
NAO index
Year
Pressure Gradient
NAO index
10
5
0
-5
3
2
1
0
-1
-2
-3
79-80
81-82
83-84
85-86
87-88
89-90
91-92
93-94
95-96

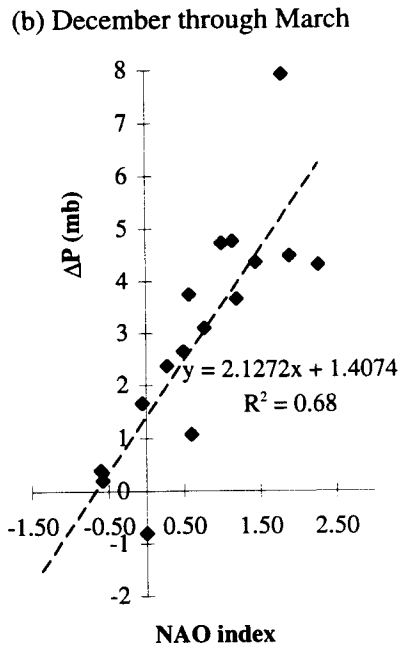
(b) December through March
ΔP (mb)
NAO index
y = 2.1272x + 1.4074
R² = 0.68
8
7
6
5
4
3
2
1
0
-1
-2
-1.50
-0.50
0.50
1.50
2.50

Fig . 11

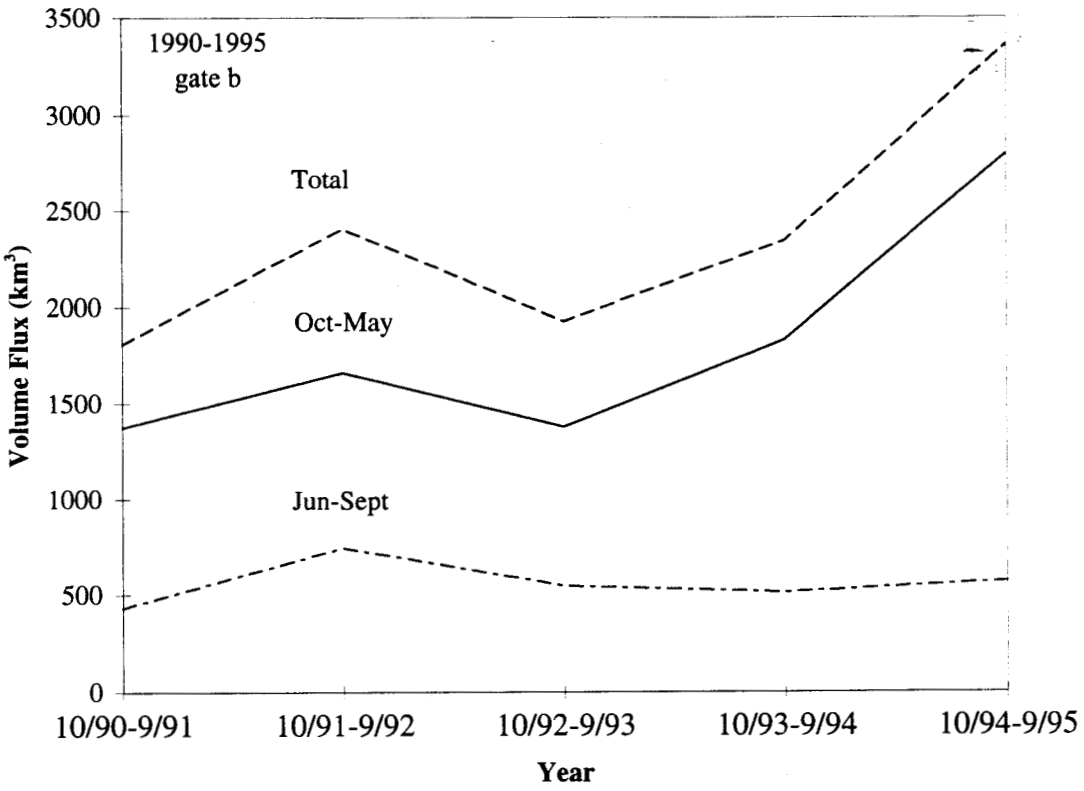
1990-1995
gate b
Total
Oct-May
Jun-Sept
Volume Flux (km³)
3500
3000
2500
2000
1500
1000
500
0
10/90-9/91
10/91-9/92
10/92-9/93
10/93-9/94
10/94-9/95
Year

Fig. 12